Journal of Simulation and Analysis of Novel Technologies in Mechanical Engineering
17 (4) (2025) 0071~0086
DOI 10.71939/jsme.2025.1222834

Research article

Structural analysis of corrugated composite shell for use in morphing structures

Behrooz Shahriari*, Mahdi Sharifi, Maryam Kazemi

Faculty of Mechanics, Malek Ashtar University of Technology, Isfahan, Iran

*shahriari@mut-es.ac.ir

(Manuscript Received --- 30 Oct. 2025; Revised --- 03 Jan. 2026; Accepted --- 06 Jan. 2026)

Abstract

Today, the use of morphing technology and corrugated composite shells as a new structure in aerospace systems has attracted the attention of researchers who want to enhance the performance of aerospace systems. In this research, using strain energy and Castigliano's theorems, the deformation of corrugated composite shells with sinusoidal, trapezoidal, square, and triangular geometries is calculated and the effect of geometric and mechanical parameters in each waveform is investigated. Among the waveforms, the sinusoidal waveform has the highest deformation and also the lowest tensile stiffness compared to other waveforms. Therefore, this waveform is further studied. First, a sinusoidal corrugated shell made of 7050 aluminum alloy is considered and compared with a glass/epoxy composite. The results show that in 7050 aluminum alloy, the change in length is 50% less than glass/epoxy composite and 62% higher in hardness. Also, the composite sinusoidal corrugated shell is investigated in terms of calculating the principal stress in all layers, to detect maximum stress points during failure. The theoretical values calculated in MATLAB software have also been compared with the results of finite element analysis in ABAQUS software. The results of this comparison indicate that the maximum stresses are in the body (66×10^6 Pa) and bottom (16×10^6 Pa) of the corrugated shell, and the minimum stress (340×10^3 Pa) is at the top of the shell.

Keywords: Composite, Corrugated shell, Morphing technology, Finite element method, Effective tensile and bending stiffness.

1- Introduction

Along with the evolution of the airplane, the science of modifying and improving its performance also developed and tremendous progress has been made in this field. The use of advanced structures in the design and construction of aircraft is recognized as one of the key factors in improving performance, increasing safety, and reducing costs in the aviation industry. With the advancement of materials and engineering technologies, new structures have emerged that have significantly improved the mechanical properties of aircraft.

Morphing structures refer to systems that can change their shape or performance in response to various environmental conditions or specific needs. These structures can change shape in response to variations in load, speed, and weather conditions, thereby optimizing their performance. This adaptability is a significant advantage in the design of modern aircraft.

In general, a morphing structure consists of two important parts, one is the structure and the other is commands and actuators. In the structure part, multi-stable structures and corrugated structures can be used, and in the commands and actuators part, memory alloys and piezo films can be used.

In this regard, research and development have started on new concepts, an example of which is the appearance of the morphing wing (adaptive wing) in the design of airplanes. A morphing aircraft wing needs to have different mechanical behavior in two directions at the same time. This type of wing should have high stiffness in the direction perpendicular to the wave to bear bending and aerodynamic loads, and it should have low stiffness in the direction of the wave for easy deformation. One of the best ways to have a morphing structure is to design it in the form of a corrugated shell in different shapes (trapezoidal, sinusoidal, etc.). Composite materials can be used to build morphing structures. Composite structures have high strength and at the same time low weight. These structures also have a high degree of anisotropy, which is suitable for use in morphing structures.

Using a morphing structure may increase the cost, complexity, and weight, but in real conditions, these structures have positive characteristics and advantages that overshadow these disadvantages. The use of corrugated shells in morphing wings in the aviation industry can bring countless benefits. Some of these advantages are increasing the performance of the structure, ease of better control (in phases such as take-off, changing the flight direction, and changing the speed), providing the best aerodynamic performance in different conditions, increasing the performance efficiency during flight, preventing the creation of unwanted aerodynamic flows, reducing the costs of the air fleet such as fuel, performing several operations at the same time, maximizing aerodynamic advantages such as increasing lift, increasing fuel economy (saving between 3 to 5 percent in fuel consumption), reducing aircraft weight, increasing efficiency and improving productivity.

Corrugated shells are widely used as structural elements in engineering fields due to their high hardness and lightweight. In addition, corrugated composite shells have attracted much attention as an option for aircraft wing deformation, which requires different behaviors in different directions. To investigate the mechanical behavior of these structures in the design process, a simple model is often needed. According to this demand, most researchers have used the method of homogenization equivalent to corrugated shells during the past decades. In this homogenization model, a corrugated shell is usually treated as an orthotropic plate, which has different mechanical properties in both horizontal and vertical directions. Kazemahvazi et al. [1,2] investigated the trapezoidal corrugated composite shells in terms of the effect of the material of the shells and focused on the trapezoidal wave compression effect. Ghabezi and Golzar [3] investigated the mechanical properties such as elasticity and hardness of a corrugated glass/epoxy composite shell in longitudinal

and transverse directions in different corrugated structures (trapezoidal, rectangular, triangular, and sinusoidal). Xia et al. [4] used homogeneous plates with different but simple geometries (sinusoidal and trapezoidal), analyzed the performance of these different geometries, and compared them with each other. Khalid [5] conducted a finite element analysis on composite corrugated shells subjected to dynamic axial crushing. Triangular, rectangular, and sinusoidal corrugation types were investigated. It was concluded that the corrugation type has a significant influence on the mean crushing load and energy absorption of corrugated shells under lateral loading. It was also concluded that the crushing load and energy absorption of glass epoxy corrugated shells were slightly higher than that of jute/epoxy corrugated shells for all corrugation types tested. Schmitz and Horst [6] investigated the influence of the geometric parameters of corrugation on deformation limits and stiffness, both experimentally and theoretically. Finally, they provided bending charts that facilitate the selection of suitable corrugation geometry during the preliminary design phase. Dayyani et al. [7] optimized the geometrical parameters of corrugated composite panels to reduce the internal stiffness and weight of the structure and increase the surface stiffness due to the bending of the corrugated shell. Takahashi et al. [8] investigated and simulated a variable camber morphing wing composed of corrugated structures. They then built the model and tested it through wind tunnel experiments. The deformations in the experimental test were correlated with the simulation results. Airoldi et al. [9] selected a set of corrugated shapes and evaluated their response using different analytical approaches. Finally, they stated the critical issues regarding the aerodynamic efficiency of corrugated skins and presented solutions for the development of a skin system based on corrugated laminates that avoids the detrimental effects on aerodynamic performance caused by corrugations. Vigliotti and Pasini [10] presented a novel lattice-based microarchitecture for the material of wing skin, characterized by very high in-plane uniaxial compliance and anisotropy. They used a nonlinear homogenization methodology to obtain a macroscopic constitutive model of the material that explains the effect of geometric nonlinearities. Finally, they compared the performance of the proposed microarchitecture with the characteristics of traditional honeycombs. Zhang et al. [11] researched about anisotropic and isotropic composites, stating general methods for investigating multistable structures with different properties, and investigating driving forces to transform one equilibrium structure into another structure (such as memory alloys, thermal, magnetic, piezoelectric, and mechanical actuators). Yang et al. [12] designed a new morphing wing capable of bending and changing shape with double driving. Their designed wing consisted of a basic structure consisting of a seven-bar mechanism as well as a corrugated sandwich shell of compressed rubber. In this regard, parameters such as the effect of different rod length ratios on the maximum extension length of the morphing wing and the effect of different actuator speeds on the maximum bending angle (under the same rod length ratio) were compared and analyzed.

Zhou et al. [13] have worked on a multi-use aircraft as a special structure that can both fly in the air and dive underwater and has a wide perspective in military applications.

They have simulated a kind of morphing wing by considering the bionic design, which can be closed when the plane is diving underwater and then open when flying in the air. Also, Bai et al. [14] also continued research in this field. Weaver-Rosen et al. [15] designed a structurally consistent camber morphing wing for light aircraft applications and analyzed it using parametric optimization techniques to maximize the lift-to-drag ratio. They concluded that parametric optimization is useful for optimizing morphing structures across a range of operating conditions. Deo and Yu [16] obtained equivalent plate properties for composite corrugated structures using mechanics of structure genome.

Nowadays, in the latest research, the control of morphing structures is also discussed more. The control of these structures can be done through changes in the material of the structure, the combination of memory alloys or the use of different controllers, as well as the use of modern sciences such as artificial intelligence and neural networks.

In this regard, Wang et al. [17] investigated the control problem for a class of morphing aircraft with telescopic wings. Their simulation results show that the designed algorithm is excellent in tracking and has guaranteed robustness and anti-saturation performance. Mkhoyan et al. [18] were able to control the structure by integrating the RBFNN[1] neural network model with an optimization strategy. Yang and Chen [19] designed a nonlinear controller for height tracking of morphing aircraft in the presence of unknown aerodynamic disturbances. They used an adaptive sliding controller in their simulation. Zucco and Weaver [20] presented a new design of multi-support corrugated shell structures on elastic walls performed high-fidelity geometric nonlinear elastoplastic analysis on it, and finally discussed the influence of plastic effects on multi-stable behavior. Mohammadi [21] analyzed the thermal buckling of corrugated trapezoidal graphene platelet reinforced composite (FG GPLRC) laminated panels. He concluded that with constant corrugation angle and amplitude when more corrugation units are added to the original panel, the critical buckling temperature difference remains almost constant. Mohammadi [22] developed an isogeometric method for free vibration analysis of trapezoidal corrugated nanocomposite laminated panels while considering the corrugation effect. Zheng et al. [23] An analytical method is proposed for flutter stability analysis of composite corrugated shells in supersonic flow. They investigated trapezoidal and sinusoidal composite corrugated shells and concluded that these shells can be used in the morphing wings. Liu et al. [24] designed a controller for a hypersonic morphing plane with the six-degree-of-freedom to maintain stability in the deformation process. Zebedee et al. [25] used optical sensors as the most reliable sensors for the morphing wing controller during flight. These sensors are in the category of piezoelectric actuators, which are the most suitable actuators for the morphing wing structure due to their weight, accuracy, and speed. Also, they used fuzzy controllers for more accurate calculations.

Considering the importance of composite corrugated shells for use in morphing technology, efforts have been made to examine all the effective parameters in different wave models in this study. To this

[1] Radial Basis Function Neural Network

end, concepts such as the degree of tensile and bending anisotropy, the effects of dimensional parameters, types of fiber textures, amplitude and step size, effective tensile and bending stiffnesses in various wave directions, and tensile, bending, and coupling stiffness matrices for shells with trapezoidal, sinusoidal, square, and triangular geometries with symmetric and asymmetric layering are investigated. Their accuracy is evaluated with the results of finite element simulation.

To apply this technology and use corrugated shells as functional structures, a sinusoidal geometrical corrugated shell made of aluminum 7050 is compared with a glass/epoxy composite in terms of tensile and bending stiffness, as well as length change.

2- Governing equations and theoretical formulation

2-1- Theory and relationships governing corrugated shells

In this research, at first, the shell is considered as a cantilever beam that has been bent under the extensive load caused by the weight. The shape change caused by the extended load in the cantilever beam is expressed as Eq. (1).

$$\delta_{max} = \frac{wL^4}{8E_1 I} \tag{1}$$

In Eq. (1), (w) is the pressure applied to the beam, (L) is the length of the beam, (E) is the Modulus of Elasticity, and (I) is the Moment of Inertia for the beam profile. Also, the deformation of each element can be calculated using the strain energy of the same element and using Castigliano's first and second theorems. Eqs. (2) and (3) represent the axial strain energy and bending strain energy, respectively, and Eq. (4) represents the total strain energy. In Eq. (2), (P) is the force applied to the beam and (A) is the cross-sectional area of the beam, and in Eq. (3), (M) is the bending moment. Tensile and bending stiffnesses (per unit width) in the longitudinal direction of corrugated shells can be calculated from Eqs. (5) and (6).

$$U_P = \int_0^l \frac{P^2}{2EA}\, ds \tag{2}$$

$$U_M = \int_0^l \frac{M^2}{2EI}\, ds \tag{3}$$

$$U_T = U_P + U_M \tag{4}$$

$$\delta = \frac{\partial U_T}{\partial P} \tag{5}$$

$$\theta = \frac{\partial U_M}{\partial P} \tag{6}$$

On the other hand, in a composite shell, the force and moment in a multilayer can be expressed as Eqs. (7) and (8) [26]. In Fig. (1), different parameters related to layering are shown.

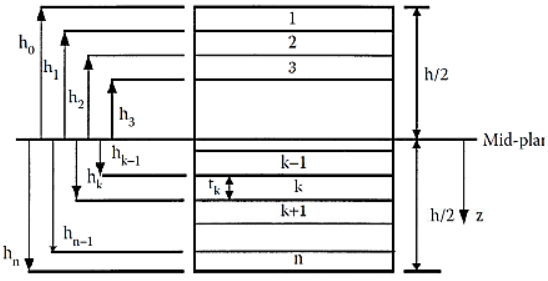

Fig. 1 Different parameters related to layers [5].

$$\begin{bmatrix} N_x \\ N_y \\ N_{xy} \end{bmatrix} = \begin{bmatrix} A_{11} & A_{12} & A_{66} \\ A_{12} & A_{22} & A_{26} \\ A_{16} & A_{26} & A_{66} \end{bmatrix} \begin{bmatrix} e_x^0 \\ e_y^0 \\ e_{xy}^0 \end{bmatrix} + \begin{bmatrix} B_{11} & B_{12} & B_{16} \\ B_{12} & B_{22} & B_{26} \\ B_{16} & B_{26} & B_{66} \end{bmatrix} \begin{bmatrix} K_x \\ K_y \\ K_{xy} \end{bmatrix} \quad (7)$$

$$\begin{bmatrix} M_x \\ M_y \\ M_{xy} \end{bmatrix} = \begin{bmatrix} B_{11} & B_{12} & B_{66} \\ B_{12} & B_{22} & B_{26} \\ B_{16} & B_{26} & B_{66} \end{bmatrix} \begin{bmatrix} e_x^0 \\ e_y^0 \\ e_{xy}^0 \end{bmatrix} + \begin{bmatrix} D_{11} & D_{12} & D_{66} \\ D_{12} & D_{22} & D_{26} \\ D_{16} & D_{26} & D_{66} \end{bmatrix} \begin{bmatrix} K_x \\ K_y \\ K_{xy} \end{bmatrix} \quad (8)$$

In Eqs. (7) and (8), the matrices (*e*) and (*K*) represent the midplane strains and midplane curvatures, respectively, and the matrices (*N*) and (*M*) represent the force and moment. Also, matrices [*A*], [*B*], and [*D*] are the extensional stiffness matrices, coupling stiffness matrices, and bending stiffness matrices in a flat shell for the lamination, respectively, which can be calculated from Eqs. (9)–(11); These equations are derived from Classical Laminate Theory (CLT) of composite materials. Eq. (12) shows the compliance matrix, which is a combination of matrices [*A*], [*B*], and [*D*].

For symmetric laminate configurations, the coupling stiffness matrix [*B*] is zero, and the extensional and bending responses are fully decoupled. For asymmetric laminates, extension–bending coupling exists due to the nonzero [*B*] matrix. In the present study, the analytical extraction of effective tensile and bending stiffnesses for asymmetric corrugated shells is performed using equivalent global stiffness measures, and the [*B*] matrix is not explicitly included in the closed-form derivations. Nevertheless, the finite element simulations inherently account for the full laminate stiffness, including coupling effects, allowing the influence of asymmetric layups to be reflected in the numerical validation results.

$$A_{ij} = \sum_{k=1}^{n} \left[\left(\overline{Q_{ij}}\right)\right]_k (h_k - h_{k-1}), \quad i = 1,2,6;\ j = 1,2,6 \quad (9)$$

$$B_{ij} = \sum_{k=1}^{n} \left[\left(\overline{Q_{ij}}\right)\right]_k (h_k^2 - h_{k-1}^2) \quad i = 1,2,6;\ j = 1,2,6 \quad (10)$$

$$D_{ij} = \sum_{k=1}^{n} \left[\left(\overline{Q_{ij}}\right)\right]_k (h_k^3 - h_{k-1}^3) \quad i = 1,2,6;\ j = 1,2,6 \quad (11)$$

$$\begin{bmatrix} N_x \\ N_y \\ N_{xy} \\ M_x \\ M_y \\ M_{xy} \end{bmatrix} = \begin{bmatrix} A_{11} & A_{12} & A_{66} & B_{11} & B_{12} & B_{16} \\ A_{12} & A_{22} & A_{26} & B_{12} & B_{22} & B_{26} \\ A_{16} & A_{26} & A_{66} & B_{16} & B_{26} & B_{66} \\ B_{11} & B_{12} & B_{16} & D_{11} & D_{12} & D_{66} \\ B_{12} & B_{22} & B_{26} & D_{12} & D_{22} & D_{26} \\ B_{16} & B_{26} & B_{66} & D_{16} & D_{26} & D_{66} \end{bmatrix} \begin{bmatrix} e_x^0 \\ e_y^0 \\ e_{xy}^0 \\ K_x \\ K_y \\ K_{xy} \end{bmatrix} \quad (12)$$

The extensional stiffness matrix [*A*] relates the resultant in-plane forces to the in-plane strains. The coupling stiffness matrix [*B*] couples the force and moment terms to the midplane strains and midplane curvatures. The bending stiffness matrix [*D*] relates the resultant bending moments to the plate curvatures.

One of the parameters that were used in the previous relations and matrices [*A*], [*B*], and [*D*] is the transferred stiffness matrix $[Q_{ij}]$. The transferred stiffness matrix also includes different parameters. These parameters include the components of the stiffness matrix, transfer matrix, and rotation matrix, which are detailed in Eqs. (13-21) [26]. (ν) in Eqs. (13-17) represents Poisson's ratio.

$$Q_{11} = \frac{E_1}{1 - \upsilon_{21}\upsilon_{12}} \quad (13)$$

$$Q_{22} = \frac{E_2}{1 - \upsilon_{21}\upsilon_{12}} \quad (14)$$

$$Q_{66} = G_{12} \quad (15)$$

$$Q_{21} = \frac{\upsilon_{21}E_1}{1 - \upsilon_{21}\upsilon_{12}} \quad (16)$$

$$Q_{12} = \frac{\upsilon_{12}E_2}{1 - \upsilon_{21}\upsilon_{12}} \quad (17)$$

$$T = \begin{bmatrix} c^2 & s^2 & 2sc \\ s^2 & c^2 & -2sc \\ -sc & sc & c^2 - s^2 \end{bmatrix} \quad (18)$$

$$[T]^{-1} = \begin{bmatrix} c^2 & s^2 & -2sc \\ s^2 & c^2 & 2sc \\ sc & -sc & c^2 - s^2 \end{bmatrix} \quad (19)$$

$$[\bar{Q}] = [T]^{-1}[Q][R][T][R]^{-1} \quad (20)$$

$$R = \begin{bmatrix} 1 & 0 & 0 \\ 0 & 1 & 0 \\ 0 & 0 & 2 \end{bmatrix} \quad (21)$$

By applying force to a corrugated shell, what happens in two existing directions (in the direction of the wave and the direction perpendicular to the waves) is that applying force in the longitudinal direction only changes the length of the corrugated shell in the longitudinal direction, but does not cause a change in the length in the transverse direction. Therefore, taking into account assumptions such as the corrugated shell not being flattened due to the application of load, $(\upsilon_{12\,eff})$ $r$elated to the corrugated shell can be considered almost equal to zero. It can also be assumed that the corresponding $(\upsilon_{21\,eff})$ is equal to the flat shell [27]. Therefore, the relations of the stiffness matrix of a corrugated shell are calculated as Eq. (22). (G) is the shear modulus.

$$[Q]_{eff} = \begin{bmatrix} E_{Leff} & \upsilon_{12}E_{Teff} \cong 0 & 0 \\ \upsilon_{21}E_{Leff} & E_{Teff} & 0 \\ 0 & 0 & G_{12\,eff} \end{bmatrix} \quad (22)$$

Now, if it is a composite corrugated shell, there is more maneuverability to change the amount of anisotropy of the structure. The concept of anisotropy can be expressed in two ways: tensile anisotropy and bending anisotropy.

Tensile anisotropy is the ratio of the effective tensile stiffness in the transverse direction to the effective tensile stiffness in the longitudinal direction in Eq. (23) and bending anisotropy is the ratio of the effective bending stiffness in the transverse direction to the effective bending stiffness in the longitudinal direction in Eq. (24). In flat shells with woven fibers, the degree of anisotropy is equal to one, while this number is very large in corrugated shells with woven fibers.

$$E^* = \frac{E_{T\,eff}}{E_{L\,eff}} \quad (23)$$

$$D^* = \frac{D_{T\,eff}}{D_{L\,eff}} \quad (24)$$

2-2- Relationships governing the sinusoidal corrugated shell

In Fig. (2), the sinusoidal element is shown as a cantilever beam, which is under tensile force and bending moment at its end. Based on Castiglione's first and second theorems, the shape change of the end of the beam can be obtained as Eq. (26) [27].

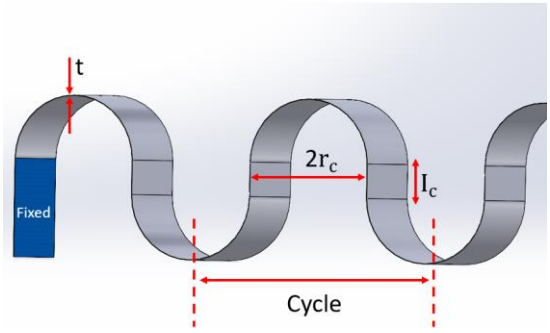

Fig. 2 Effective parameters in the sinusoidal element.

In general, the shape change in a corrugated shell under axial load can be written according to Eq. (25).

$$\delta = \frac{PL}{A_{eff}E_{Leff}} \tag{25}$$

where (A_{eff}) is the cross-sectional area equivalent to the surface. By obtaining the strain energy in the sinusoidal element, the shape change of the end of the shown beam can be obtained according to Eq. (26).

$$\delta = \frac{P}{D_{11}}\left(\frac{I_C^3}{3} + r_C\left\{\frac{\pi}{4}(2I_C^2 + r_C^2) + 2I_C r_C\right\}\right) \tag{26}$$

By setting the right side of Eqs. (25) and (26) equal, the equivalent tensile stiffness in the wave direction for a pseudo-sinusoidal shell can be obtained as Eq. (27) [27,28].

$$E_{Leff} = \frac{r_C D_{11}}{h_C\left[\frac{I_C^3}{3} + r_C\left\{\frac{\pi}{4}(2I_C^2 + r_C^2) + 2I_C r_C\right\}\right]} \tag{27}$$

where (h_c) is equal to the wave amplitude. By obtaining the strain energy resulting from the application of the bending moment and using the previous relations, it is possible to calculate the angle change of the end of the sinusoidal element according to Eq. (28).

$$\theta = \frac{M}{D_{11}}\left(\frac{\pi}{2}r_C + I_C\right) \tag{28}$$

On the other hand, the angle change at the end of a flat shell can be expressed as Eq. (29).

$$\theta = \frac{ML}{D_{Leff}} \tag{29}$$

Now, by setting the sides of Eqs. (28) and (29) equal, the equivalent bending stiffness in the transverse direction per unit width for a sinusoidal shell was obtained according to Eq. (30) [27,28].

$$D_{Leff} = \frac{LD_{11}}{r_C\frac{\pi}{2} + I_C} \tag{30}$$

By obtaining the equivalent area and the moment of inertia of the surface in the transverse direction of the corrugated shell, the tensile and bending stiffnesses in the transverse direction of the shell can be obtained. Also, the deformation caused by the axial load in the transverse direction of the corrugated shell can be equated with the deformation of the flat shell in the transverse direction, and by placing the cross-section of the flat shell and the sinusoidal corrugated shell and then simplifying, the equivalent tensile stiffness in the transverse direction can be reached in Eq. (37). Eqs. (31-36) shows the values required in Eq. (37).

$$\delta = \frac{PL}{AE_2} \tag{31}$$

$$\delta = \frac{PL}{A_{eff}E_{Teff}} \tag{32}$$

$$A = (2\pi r_c + 4I_C)t \tag{33}$$

$$A_{eff} = h_c w_C \tag{34}$$

$$w_C = 4r_c \tag{35}$$

$$h_c = 2(r_c + I_C) + t \tag{36}$$

$$E_{Teff} = \frac{2\pi r_c + 4I_C}{h_c w_C} A_{22} \tag{37}$$

In Eq. (37), the width and height of the sinusoidal corrugated shell are calculated [27]. By applying the bending moment in the transverse direction of the corrugated shell and making its deformation equal (Eq. 38) to the deformation of the equivalent flat shell (Eq. 39), the equivalent bending stiffness in the transverse direction per unit width can be expressed as Eq. (40) [27,28]. In these relationships, (E_1) and (E_2) Young's modulus corresponds to the flat shell in the longitudinal and transverse directions, respectively.

$$\delta = \frac{ML^2}{2E_2 I} \tag{38}$$

$$\delta_{eff} = \frac{ML^2}{2D_{Teff}} \tag{39}$$

$$D_{Teff} = \frac{A_{22}(24\pi r_c I_C^2 + 16I_C^3)}{48r_c} + \frac{A_{22}\left(3\pi r_c(4r_C^2 + t^2) + 8I_C(12r_C^2 + t^2)\right)}{48r_c} \tag{40}$$

Similarly, for trapezoidal, square, and triangular corrugated shells, the effective bending and tensile stiffness can be calculated in both longitudinal and transverse directions (Fig. 3).

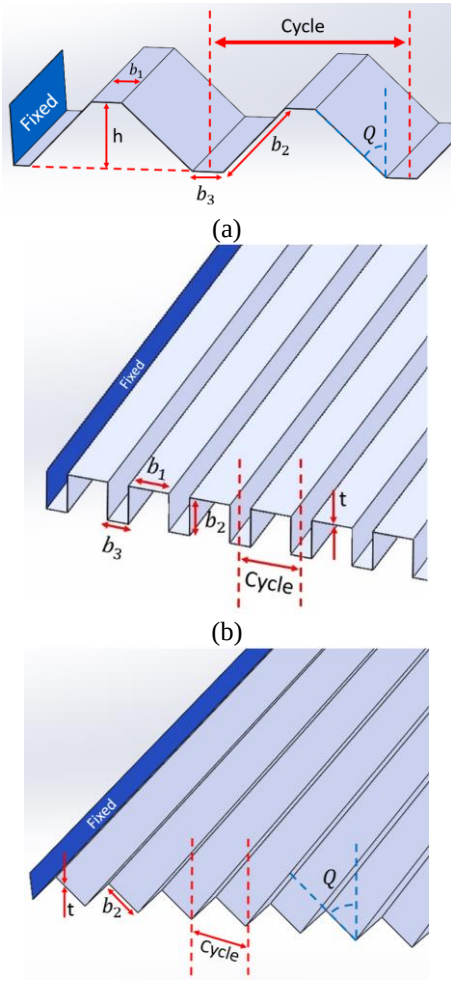

Fig. 3 Effective parameters in (a) trapezoidal, (b) square, and (c) triangular corrugated shells.

3- Simulation, review, and analysis of results

The finite element simulations were carried out using Abaqus/Standard under static loading conditions. The corrugated shell was modeled as a cantilever structure, where one end of the shell was fully constrained by fixing all translational and rotational degrees of freedom to represent a clamped boundary condition. A uniformly distributed load was applied along the longitudinal direction of the shell, consistent with the analytical assumptions used in the strain energy and Castigliano-

based formulations. The applied load magnitude corresponded to the values reported in Table 1. The finite element mesh consisted of quadrilateral shell elements with an average element size of 0.5 mm. This mesh size was selected based on mesh sensitivity considerations and previous studies on corrugated composite shells reported in the literature [3,7,28]. A finer discretization was used in regions with high curvature to adequately capture stress gradients.

In this part, by using the obtained theoretical relations, changing the effective dimensional parameters in each waveform, as well as changing the arrangement of layers and thickness, these shells were investigated from different directions such as tensile and bending stiffness in longitudinal and transverse directions, and the amount of deformation (strain). Tables (1) and (2) respectively represent the general mechanical characteristics of the investigated shells, the process of changing the effective parameters in each waveform, and the general results of changing these parameters in each waveform.

Table 1: Mechanical, physical, and dimensional characteristics of corrugated shells.

Material	E (GPa)		V	G (GPa)			Density (g/cm^3)	Tensile Strength (MPa)	Yield Strength (MPa)
	E_1	E_2	V_{12}	G_{12}	G_{13}	G_{23}			
Glass/epoxy	38.6	8.27	0.3	4.14	4.1	1.5	2.6	479.9	479.9
Aluminum alloy 7050	70.3		0.33		26.9		2.3	515	455

Dimensions of shells	L (mm)	W (mm)	t (mm)	P (N)	M (N.mm)	Arrangement of shells	Weight of each layer (kg)
	250	25	0.7	20000	613.125	$[0/0/90]$ $[30/30/90]$ $[0/90/\bar{0}]_S$	0.1

Table 2: Comparison of effective parameters in corrugated shells.

Corrugated shells	With increasing	E_L	E_T	D_L	D_T	E^* (E_T/E_L)	D^* (D_T/D_L)	Length change (strain)
Sinusoidal	I_C	Decrease	Decrease	Increase	Increase	Increase	Increase	Decrease
	r_c	Decrease	Decrease	Decrease	Increase	Increase	Increase	Decrease
Trapezoidal	b_2	Decrease	Decrease	Increase	Increase	Increase	Increase	Increase
	b_1,b_3	Decrease	Decrease	Decrease	Increase	Decrease	Decrease	Increase
	Q	Increase	Increase	Increase	Decrease	Decrease	Decrease	Decrease
Square	b_2	Decrease	Decrease	Decrease	Increase	Increase	Increase	Increase
	b_1,b_3	Increase	Decrease	Increase	Decrease	Decrease	Decrease	Increase
Triangular	b_2	Decrease	Decrease	Decrease	Increase	Increase	Increase	Increase
	Q	Increase	Increase	Increase	Decrease	Decrease	Decrease	Increase
Thickness effect	t	Increase	Increase	Increase	Increase	Decrease	Decrease	Decrease

Also, the diagrams in Fig. (4), summarize the ranking between the highest and the lowest bending and tensile stiffness in the longitudinal and transverse directions between different waveforms.

The mechanical characteristics of the sinusoidal waveform in the symmetrical and asymmetrical arrangements are also investigated in Table (3).

Fig. 4 Comparison of mechanical properties of corrugated shells.

Table 3: Comparing symmetrical and asymmetrical layering.

Corrugated shells	Arrangement	Thickness (mm)	E_L(MPa)	E_T(MPa)	D_L(N.m)	D_T(N.m)	E* (E_T/E_L)	D* (D_T/D_L)
Sinusoidal	$[0/90/\bar{0}]_S$	0.7	1.8	2484	0.5	863	1310	1520
	[0/0/90]	0.3	9.5	771	0.027	260	81.03	9354
	[30/30/90]	0.3	6.9	845	0.020	285	121	14046

Aluminum and its various alloys are heavily used in the construction of airplanes and aerial structures due to their high strength, low weight, and high corrosion resistance. The top choice for aerospace applications is aluminum alloy 7050, which exhibits much higher corrosion resistance than other alloys. Therefore, in this section, aluminum alloy 7050 was investigated for comparison with glass/epoxy composite (Fig. 5).

According to Fig. (5), it can be concluded that the tensile and bending stiffness in the longitudinal and transverse directions of aluminum alloy 7050 corrugated shells is higher than glass/epoxy composite corrugated shells. Also, the amount of

length change in these shells is less. To predict fiber failure, the amount of principal stresses in each layer can be calculated by using the principal stresses of glass/epoxy composite with unidirectional fibers (Table 1 and 2 in reference [12]) and related relationships. Consequently, as shown in Fig. (6), the difference in maximum principal stress between theory and simulation methods is 2.12% in the longitudinal direction and 11.77% in the transverse direction.

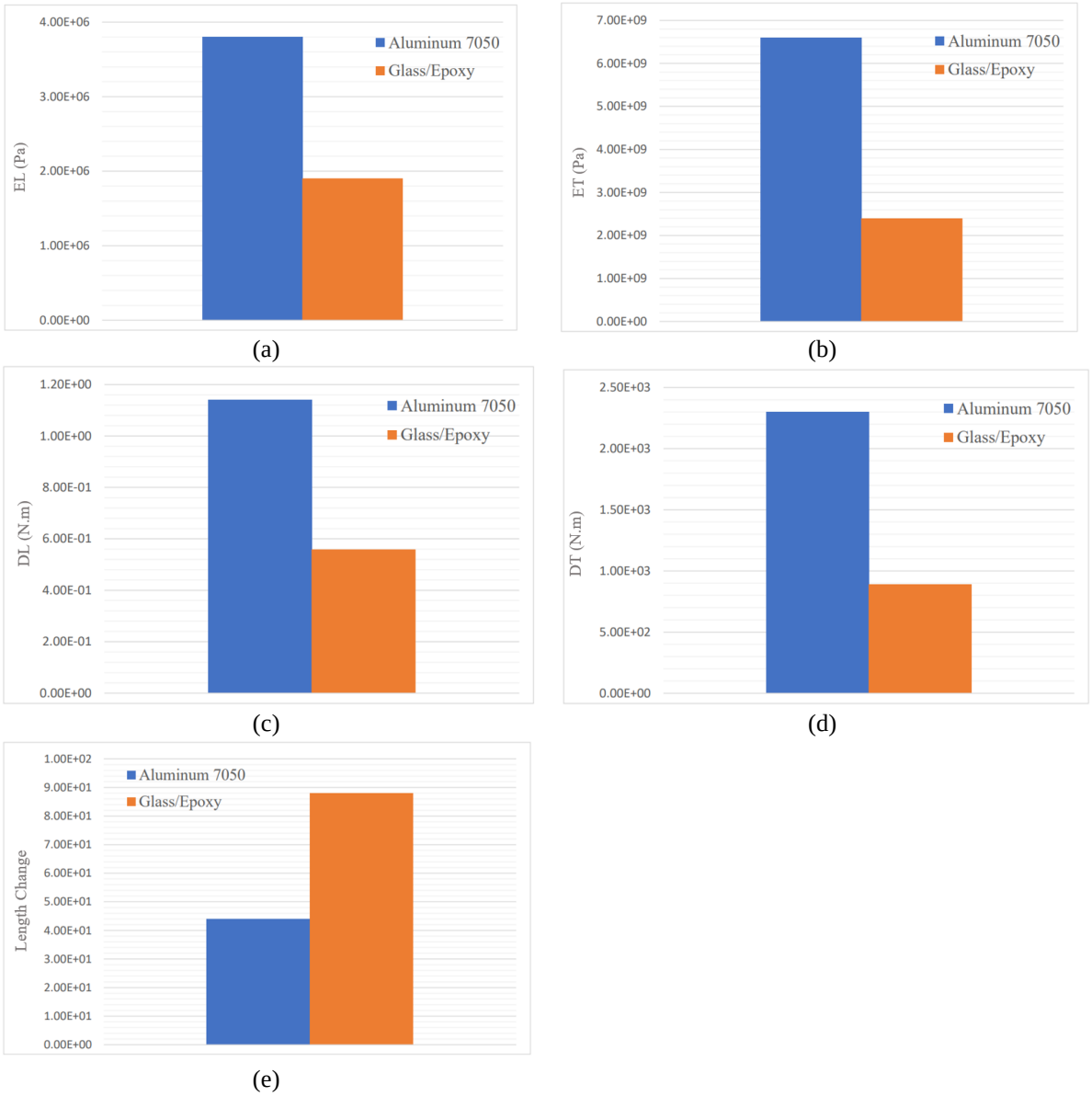

Fig. 5 Comparison of aluminum alloy 7050 with glass/epoxy composite in terms of (a) tensile strength in the longitudinal, (b) tensile strength in the transverse, (c) bending stiffness in the longitudinal, (d) bending stiffness in the transverse, and (e) length change.

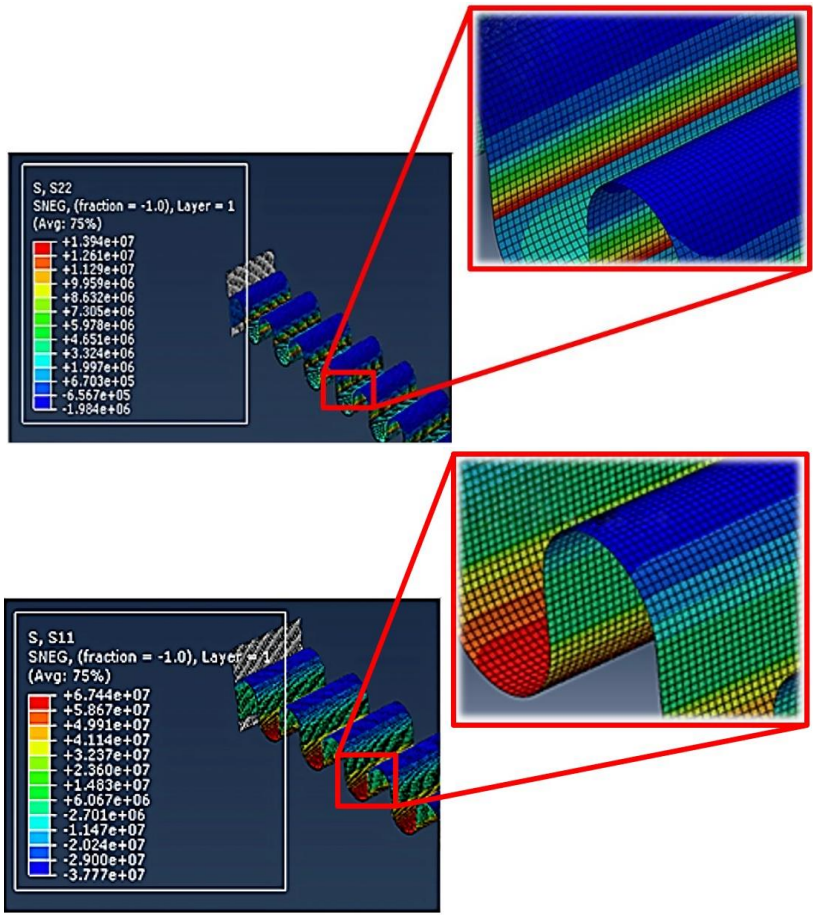

	σ_1	σ_2	σ_{12}
TOP	-3.40E+05	7.32E+06	0.00E+00
MID	-3.85E+05	8.17E+06	0.00E+00
BOTT	-4.30E+05	9.02E+06	0.00E+00
TOP	4.21E+07	4.11E+05	0.00E+00
MID	4.61E+07	4.49E+05	0.00E+00
BOTT	5.01E+07	4.86E+05	0.00E+00
TOP	-5.20E+05	1.07E+07	0.00E+00
MID	-5.65E+05	1.16E+07	0.00E+00
BOTT	-6.09E+05	1.24E+07	0.00E+00
TOP	5.80E+07	5.62E+05	0.00E+00
MID	6.20E+07	6.00E+05	0.00E+00
BOTT	6.60E+07	6.38E+05	0.00E+00
TOP	-6.99E+05	1.41E+07	0.00E+00
MID	-7.44E+05	1.50E+07	0.00E+00
BOTT	-7.89E+05	1.58E+07	0.00E+00

Fig. 6 Comparison of principal stresses of sinusoidal corrugated shell in MATLAB and ABAQUS software.

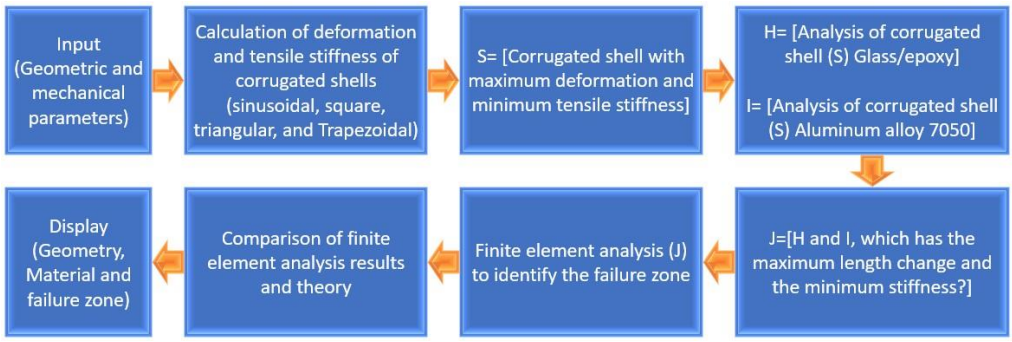

Fig. 7 General flowchart for analysis steps.

The study conducted included steps to select the best geometry, material, and determine the zone of the failure. The flowchart of these steps is presented in Fig. (7).

4- Conclusion

Using the obtained theoretical relations, changing the different dimensional parameters effective in each waveform, and changing the arrangement of layers and thickness, these shells were investigated from different aspects such as tensile and bending stiffness in the longitudinal and transverse directions and the amount of deformation. The effect of thickness in all waveforms was such that the amount of strain and deformation in the shells decreased with the increase in thickness. Also, among the different waveforms, the sinusoidal waveform had the largest change in length (strain), and after that, square, triangular, and trapezoidal waveforms had the largest deformation (strain). In this regard, by examining symmetric and asymmetric arrangements in the sinusoidal waveform, it was concluded that in the case of symmetric arrangement ($[0/90/\bar{0}]_S$) The tensile and bending anisotropy are in a close range (1310) and (1520) respectively. Whereas in the asymmetric arrangement ([0/0/90]), there is a huge difference between the tensile and bending anisotropy; the tensile anisotropy (81.03 Pa) is much less than the bending anisotropy (9354 Pa). Also, in the comparison between the two investigated alloys, glass/epoxy, and aluminum 7050, the results showed that the tensile stiffness in the longitudinal direction (4×10^6 Pa), the bending stiffness in the longitudinal direction (1), the tensile stiffness in the transverse direction (6×10^9 Pa), and the bending stiffness in the transverse direction (25×10^2 Pa) were about twice more in aluminum 7050 than that of glass/epoxy. Therefore, the length change in aluminum alloy 7050 is less and about half of glass/epoxy, which is not recommended for use in morphing structures compared to glass/epoxy.

Finally, the sinusoidal corrugated shell made of glass/epoxy composite materials with 0-degree and 90-degree lamination was analyzed using the finite element method in ABAQUS software. It was concluded that in the layering with an angle of 0 degrees, the principal stresses are high in the longitudinal direction and this value reaches its maximum value in the lower layer. In the layering with an angle of 90 degrees, the principal stresses are high in the transverse direction and this value reaches its maximum value in the lowest layer. The results also showed that the highest stresses occur in the body (66×10^6 Pa) and the lower layer (16×10^6 Pa), and the minimum stress occurs in the upper layer (340×10^3 Pa), so there is a possibility of

layer failure in areas where the stress is maximum.

References

[1] Kazemahvazi, S., and Zenkert, D. (2009). Corrugated all-composite sandwich structures. Part 1: Modeling. Composites Science and Technology 69, 913-919.

[2] Kazemahvazi, S., Tanner, D., and Zenkert, D. (2009). Corrugated all-composite sandwich structures. Part 2: Failure mechanisms and experimental program. Composites Science and Technology 69, 920-925.

[3] Ghabezi, P., and Golzar, M. (2011). Corrugated Composites as Flexible Structures Theory and FEM Analysis. 32th Riso International Symposium on Materials Science.

[4] Xia, Y., Friswell, M.I., and Flores, E.S. (2012). Equivalent models of corrugated panels. International Journal of Solids and Structures 49, 1453-1462.

[5] Khalid, A. (2014). The behavior of composite corrugated plates subjected to lateral loading. 5th Brunei International Conference on Engineering and Technology (BICET 2014).

[6] Schmitz, A., and Horst, P. (2014). Bending deformation limits of corrugated unidirectionally reinforced composites. Composite Structures 107, 103-111.

[7] Dayyani, I., Shaw, A., Flores, E.S., and Friswell, M. (2015). The mechanics of composite corrugated structures: A review with applications in morphing aircraft. Composite Structures 133, 358-380.

[8] Takahashi, H., Yokozeki, T., and Hirano, Y. (2016). Development of variable camber wing with morphing leading and trailing sections using corrugated structures. Journal of Intelligent Material Systems and Structures 27, 2827-2836.

[9] Airoldi, A., Sala, G., Di Landro, L.A., Bettini, P., and Gilardelli, A. (2018). Composite corrugated laminates for morphing applications. In Morphing Wing Technologies, (Elsevier), pp. 247-276.

[10] Vigliotti, A., and Pasini, D. (2018). The design of skin panels for morphing wings in lattice materials. In Morphing Wing Technologies, (Elsevier), pp. 231-246.

[11] Zhang, Z., Li, Y., Yu, X., Li, X., Wu, H., Wu, H., Jiang, S., and Chai, G. (2019). Bistable morphing composite structures: A review. Thin-walled structures 142, 74-97.

[12] Yang, G., Guo, H., and Liu, R. (2019). Design and Analysis of a Variable-Span and Cambered Span Morphing Wing for UAV. 2019 IEEE International Conference on Robotics and Biomimetics (ROBIO), 1318-1324.

[13] Zhou, H., Plummer, A.R., and Cleaver, D. (2021). Distributed actuation and control of a tensegrity-based morphing wing. IEEE/ASME Transactions on Mechatronics 27, 34-45.

[14] Bai, X., Xing, X., Liu, L., Zhang, J., Ling, C., and Li, Z. (2020). Design of a Trans-Media aircraft morphing wing structure. 2020 2nd International Conference on Artificial Intelligence and Advanced Manufacture (AIAM), 33-37.

[15] Weaver-Rosen, J.M., Leal, P.B., Hartl, D.J., and Malak Jr, R.J. (2020). Parametric optimization for morphing structures design: application to morphing wings adapting to changing flight conditions. Structural and Multidisciplinary Optimization 62, 2995-3007.

[16] Deo, A., and Yu, W. (2021). Equivalent plate properties of composite corrugated structures using mechanics of structure genome. International Journal of Solids and Structures 208, 262-271.

[17] Wang, Z., Hou, M., and Hao, M. (2021). Robust composite control of telescopic wing morphing aircraft with control allocation. 2021 China Automation Congress (CAC), 67-72.

[18] Mkhoyan, T., Ruland, O., De Breuker, R., and Wang, X. (2022). On-line black-box aerodynamic performance optimization for a morphing wing with distributed sensing and control. IEEE Transactions on Control Systems Technology 31, 1063-1077.

[19] Yang, J., and Chen, F. (2023). Adaptive Backstepping Sliding Mode Control of Morphing Aircraft with Unknown Disturbances. 2023 6th International Symposium on Autonomous Systems (ISAS), 1-6.

[20] Zucco, G., and Weaver, P.M. (2023). Design of Isotropic Morphing Multi-stable Corrugated

Shell Structures on Elastic Walls. AIAA SCITECH 2023 Forum, 2227.

[21] Mohammadi, H. (2023). Isogeometric approach for thermal buckling analysis of FG graphene platelet reinforced composite trapezoidal corrugated laminated panels. Engineering Analysis with Boundary Elements 151, 244-254.

[22] Mohammadi, H. (2023). Isogeometric free vibration analysis of trapezoidal corrugated FG-GRC laminated panels using higher-order shear deformation theory. Structures 48, 642-656.

[23] Zheng, Y., Wang, Y., Huang, J., and Tan, Z. (2024). Flutter stability analysis of composite corrugated plates in supersonic flow. Archive of Applied Mechanics 94, 1079-1098.

[24] Liu, H., Zhang, Q., Cui, L., Han, X., and Yu, Y. (2022). Attitude control of hypersonic morphing aircraft based on incremental backstepping sliding mode. 2022 7th International Conference on Intelligent Computing and Signal Processing (ICSP), 1324-1331.

[25] Zebedee, E.A., Mohammed, A., and Lawal, M.S. (2019). Towards Morphing Wing Technology in Aircraft for Improved Flight Performance. 2019 2nd International Conference of the IEEE Nigeria Computer Chapter (NigeriaComputConf), 1-5.

[26] Kaw, A.K. (2005). Mechanics of composite materials, 2nd Edition Edition (CRC press).

[27] Ghabezi, P., and Golzar, M. (2011). Corrugated Composites as Flexible Structures Theory and FEM Analysis.

[28] Yokozeki, T., Takeda, S.-i., Ogasawara, T., and Ishikawa, T. (2006). Mechanical properties of corrugated composites for candidate materials of flexible wing structures. Composites Part A: applied science and manufacturing 37, 1578-1586.